Group theory analysis of early-time scale-dependent dynamics of the Rayleigh-Taylor instability with time varying acceleration

Desmond L. Hill, Aklant K. Bhowmick, Dan V. Ilyin, and Snezhana I. Abarzhi

Phys. Rev. Fluids **4**, 063905 — Published 21 June 2019

DOI: 10.1103/PhysRevFluids.4.063905

Group theory analysis of early-time scale-dependent dynamics of Rayleigh-Taylor instability with time varying acceleration

Des L. Hill (1); Aklant K. Bhowmick (2); Snezhana I. Abarzhi* (1)

The University of Western Australia, AUS (1); Carnegie Mellon University, USA (2)

*corresponding author: snezhana.abarzhi@gmail.com

We consider the long-standing problem of Rayleigh-Taylor instability with variable acceleration, and focus on the early-time scale-dependent dynamics of an interface separating incompressible ideal fluids of different densities subject to an acceleration being a power-law function of time for a spatially extended three-dimensional flow periodic in the plane normal to the acceleration with symmetry group p6mm. By employing group theory and scaling analysis, we discover two distinct sub-regimes of the early time dynamics depending on the exponent of the acceleration power-law. The time-scale and the early-time dynamics are set by the acceleration for exponents greater than -2, and by the initial growth-rate (due to, e.g., initial conditions) for exponents smaller than -2. At the exponent value (-2) a transition occurs from one sub-regime to the other with varying acceleration strength. For a broad range of the acceleration parameters, the instability growth-rate is explicitly found, the dependence of the dynamics on the initial conditions is investigated, and theory benchmarks are elaborated.

Keywords: Rayleigh-Taylor instability, coherent structures, interfacial mixing, variable acceleration

PACS: 47.20.Ma, 47.20.-k, 52.35.-g, 52.35.Py

Section 1 - Introduction

Rayleigh-Taylor instability (RTI) controls a broad range of processes in nature and technology, in fluids, plasmas and materials [1,2]. RTI develops when the fluids of different densities are accelerated against their density gradients [3,4]. Intense interfacial Rayleigh-Taylor (RT) mixing of the fluids ensues with time [1,2]. Examples of RT-relevant processes include inertial confinement fusion, supernova explosion, material transformation under impact, as well as fossil fuel recovery and nano-electronics [1,2]. In realistic environments RTI is often driven by variable acceleration, whereas the bulk of existing studies is focused on the cases of sustained and impulsive accelerations [1,2]. The case of impulsive acceleration induced by a steady shock is referred as Richtmyer-Meshkov (RM) instability [5,6]. In this work we consider the long-standing problem of RTI subject to an acceleration being a power-law function of time [1,2,7]. We focus on the early-time dynamics, and, by applying group theory and scaling analysis [7-9], identify the instability growth-rate for a broad range of acceleration parameters and initial conditions. We find two sub-regimes depending on the acceleration exponent - acceleration-driven RT-type and initial-growth-rate-driven RM-type, with each sub-regime having its own time-scale, type of dynamics, and theory benchmarks.

RT flows, while occurring in vastly different physical circumstances, have some similar features of the evolution [9]. RTI starts to develop when the fluid interface (or, the flow fields) is (are) slightly perturbed near the equilibrium state [3,4]. Over time the interface is transformed to a composition of small-scale shear driven vortical structures and a large-scale coherent structure of bubbles and spikes, with the bubble (spike) being a portion of the light (heavy) fluid penetrating the heavy (light) fluid [8]. Eventually, the flow transits to the stage of intensive interfacial mixing [7].

Non-equilibrium RT dynamics is extremely challenging to study due to, e.g., tight requirements on the flow control and diagnostics in experiments, the need to track interfaces and capture small-scale processes in simulations, the necessity to account for the non-local and singular character of the dynamics in theory [1,2]. Remarkable success has been recently achieved in understanding of the fundamentals of RTI and RT mixing [1,2,7-16]. In particular, the group theory approach has found that nonlinear RTI has a multi-scale character and that RT mixing with constant acceleration may keep order, thus explaining the observations [7-10].

A number of important aspects of RT dynamics still require a deeper understanding. One of them is variable acceleration. RT flows with variable accelerations occur commonly in nature and technology [1,2]. These include RTI induced by unsteady shocks in inertial confinement fusion, blast-wave-driven RT mixing in core-collapse supernovae, RT-unstable plasma irregularities in the Earth's ionosphere, and fossil fuel recovery in industry [17-22]. RTI and RT mixing with variable acceleration is a long-standing

problem [1,2]. Only limited information is currently available on RT dynamics under these conditions [22-24].

Here we consider RTI subject to variable acceleration with power-law time dependence. On the side of fundamentals, power-law functions are important to study because they may result in new invariant and scaling properties of the dynamics [25,26]. On the side of applications, power-law functions can be used to adjust the acceleration's time-dependence in realistic environments and thus ensure practicality of our results [17-21]. We consider a three-dimensional spatially extended periodic flow, apply group theory and scaling analysis [7,8], identify the dependence of the instability growth-rate on the acceleration's exponent and strength, and elaborate theory benchmarks for observations. Particularly, we find that the early-time dynamics is set by the acceleration for acceleration exponents greater than -2, and by the initial growth-rate for acceleration exponents smaller than -2, and that at the exponent value (-2) the transition occurs between the sub-regimes by varying the acceleration strength [22-24].

Section 2 – Method

Sub-section 2.1 - Governing equations

The dynamics of ideal fluids is governed by conservation of mass, momentum and energy:

$$\begin{aligned}
&\frac{\partial \rho}{\partial t}+\frac{\partial \rho v_i}{\partial x_i}=0,\\
&\frac{\partial \rho v_i}{\partial t}+\sum\nolimits_{j=1}^{3}\frac{\partial \rho v_i v_j}{\partial x_i}+\frac{\partial P}{\partial x_i}=0,\\
&\frac{\partial E}{\partial t}+\frac{\partial (E+P)v_i}{\partial x_i}=0 \qquad\qquad (1.1)
\end{aligned}$$

where $(x_1,x_2,x_3)=(x,y,z)$ are the spatial coordinates with, t is time, $(\rho,\mathbf{v},P,E)$ are the fields of density ρ, velocity $\mathbf{v}$, pressure P and energy $E=\rho\left(e+\mathbf{v}^2/2\right)$, e is the specific internal energy [25].

We introduce a continuous local scalar function $\theta(x,y,z,t)$, whose derivatives $\dot{\theta}$ and $\nabla\theta$ exist (the dot marks a partial time-derivative), such that $\theta=0$ at the interface, and the heavy (light) fluid is located in the region $\theta>0$ ($\theta<0$); its fields are $(\rho,\mathbf{v},P,E)\rightarrow(\rho,\mathbf{v},P,E)_{h(l)}$ and are marked with the subscript $h(l)$ hereafter [7,8,24,32]. By using the Heaviside step-function $H(\theta)$, we represent in the fluid fields in the entire domain as $(\rho,\mathbf{v},P,E)=(\rho,\mathbf{v},P,E)_h H(\theta)+(\rho,\mathbf{v},P,E)_l H(-\theta)$ [7,8,24,32]. At the interface, the balance of fluxes of mass and normal and tangential components of momentum and energy obey the boundary conditions:

$$\left[\tilde{\mathbf{j}}\cdot\mathbf{n}\right]=0,\quad \left[\left(P+\frac{\left(\tilde{\mathbf{j}}\cdot\mathbf{n}\right)^2}{\rho}\right)\mathbf{n}\right]=0,\quad \left[\left(\tilde{\mathbf{j}}\cdot\mathbf{n}\right)\left(\frac{\left(\tilde{\mathbf{j}}\cdot\boldsymbol{\tau}\right)}{\rho}\right)\boldsymbol{\tau}\right]=0,\quad \left[\left(\tilde{\mathbf{j}}\cdot\mathbf{n}\right)\left(W+\frac{\tilde{\mathbf{j}}^2}{2\rho^2}\right)\right]=0 \quad (1.2)$$

where $[...]$ denotes the jump of a quantity across the interface; $\mathbf{n}$ and $\boldsymbol{\tau}$ are the normal and tangential unit vectors of the interface with $\mathbf{n}=\nabla\theta/|\nabla\theta|$ and $(\mathbf{n}\cdot\boldsymbol{\tau})=0$; $\tilde{\mathbf{j}}=\rho\left(\mathbf{n}\dot{\theta}/|\nabla\theta|+\mathbf{v}\right)$ is the mass flux across the moving interface; the specific enthalpy is $W=e+P/\rho$ [7,8,24,25,32].

The boundary conditions Eqs.(1.2) are derived from the governing equations Eqs.(1.1) assuming that the mass flux is conserved at the interface, $\left[\tilde{\mathbf{j}}\cdot\mathbf{n}\right]=\left[\tilde{j}_n\right]=0$, with $\tilde{j}_n=\tilde{\mathbf{j}}\cdot\mathbf{n}$. There is the important particular case, when the mass flux is conserved at the interface and when it is zero at the interface, $\tilde{j}_n\big|_{\theta=0^{\pm}}=0$. This case corresponds to a so-called contact discontinuity, or a front, between, and describes the interface between two immiscible fluids [7,8,24,25,32]. As is seen from Eqs.(1.2), this special condition $\tilde{j}_n\big|_{\theta=0^{\pm}}=0$ leads to the continuity of normal component of velocity at the interface $[\mathbf{v}\cdot\mathbf{n}]=0$, and transforms the condition for the conservation of normal component of momentum at the interface to the continuity of pressure at the interface, $[P]=0$. Moreover, for the zero mass flux at the interface, $\tilde{j}_n\big|_{\theta=0^{\pm}}=0$, the condition of continuity of tangential component of momentum at the interface holds true for an arbitrary jump of the tangential velocity at the interface $[\mathbf{v}\cdot\boldsymbol{\tau}]=arbitrary$, whereas the condition of continuity of the energy flux at the interface holds true for any jump of the enthalpy at the interface $[W]=arbitrary$. Hence, in full consistency with the classic results [25], in case of zero mass flux at the interface, $\tilde{j}_n\big|_{\theta=0^{\pm}}=0$, the boundary conditions at the interface are

$$[\mathbf{v}\cdot\mathbf{n}]=0,\quad [P]=0,\quad [\mathbf{v}\cdot\boldsymbol{\tau}]=arbitrary,\quad [W]=arbitrary \qquad (2)$$

The flow is periodic in the plane (x,y) normal to the z direction of the acceleration $\mathbf{g}$, $|\mathbf{g}|=g$ [7,8], Figure 1. The acceleration is directed from the heavy to the light fluid, $\mathbf{g}=(0,0,-g)$, and is a power-law functions of time, $g=Gt^a$, $t>0$. Here a is the acceleration exponent, $a\in(-\infty,+\infty)$, and G is the pre-factor, $G>0$; their dimensions are $[G]=m/s^{2+a}$ and $[a]=1$ [22-24]. In the presence of acceleration $\mathbf{g}$, the pressure is modified as $P\to P-\rho gz$ [7,8,24]. The flow is free from mass sources:

$$\mathbf{v}\big|_{z\to+\infty}=0,\quad \mathbf{v}\big|_{z\to-\infty}=0 \quad (3)$$

The initial conditions are initial perturbations of the flow's fields. We consider incompressible fluids with negligible stratification and density variations. The spatial period (wavelength) λ of the initial perturbation sets the dynamics' length-scale [25,27-30]. The Atwood number $A=(\rho_h-\rho_l)/(\rho_h+\rho_l)$ parameterizes the ratio of the fluids' densities, with $A\to 1\,(0)$ for $(\rho_l/\rho_h)\to 0\,(1)$.

Sub-section 2.2 – Group theory for Rayleigh-Taylor dynamics

To solve the problem of RTI with variable acceleration, group theory can be employed [7,8,30]. For spatially periodic flows, space groups can be applied, since RT dynamics is invariant with respect to a group $\mathbf{G}$, whose generators are translations in the plane, rotations and reflections [7,8,24,33,34]. These groups are also known as Fedorov and/or Schoenflies groups, and they are commonly used in physics [7,8,24,25,30,33,34]. Figure 2 presents sample patterns for one-dimensional space space group $pm11$ in case of two-dimensional (2D) flow, and two-dimensional space groups $p4mm, p6mm$ in case of a three-dimensional (3D) flow. We use international classification [25,33]. Here p stands for periodicity in one (two) direction(s), and, for each of spatial directions, 1 is for unit element, m is for mirror plane of reflection, and $n=4,6$ is for n-fold axis of rotation [7,8,24,33]. While there are 7 one-dimensional and 17 two-dimensional space groups, only some of these groups should be considered, Figure 2. Particularly, groups relevant to structurally stable RT dynamics must have anisotropy in the acceleration direction and inversion in the normal plane, such as groups of hexagon $p6mm$ or square $p4mm$ for a three-dimensional (3D) flow, and group $pm11$ in a two-dimensional (2D) flow [7,8,24,25,30,33,34].

By using the techniques of group theory, we apply irreducible representations of a relevant group to expand the flow fields as Fourier series, including Fourier series of the velocity and pressure fields and the interface, and further make spatial expansions in a vicinity of a regular point at the interface (i.e., the tip of the bubble or spike). The governing equations are thus reduced to a dynamical system in terms of surface variables and moments, and the solution is sought [7,8,22-24]. We focus on the large-scale coherent dynamics with length scale $\sim\lambda$, presuming that length scale of shear-driven interfacial vortical structures is small, $<<\lambda$. For convenience, all derivations are performed in the frame of reference moving with velocity $v(t)$ in the *z*-direction, where $v(t)$ is the bubble (spike) tip velocity in the laboratory frame of references [7,8,22-24].

Sub-section 2.3 – Fourier series and spatial expansions for group $p6mm$

For the large-scale coherent structure, the fluid motion is potential, and the velocity of the heavy (light) fluid is $\mathbf{v}_{h(l)} = \nabla\Phi_{h(l)}$. For incompressible ideal fluids the equation for the conservation of mass in Eqs.(1.1) leads to the Laplace equation $\Delta\Phi_{h(l)} = 0$ in the bulk(s) for $\theta > 0\,(<0)$ [7,8,30]. Here we consider a three-dimensional structure with space group $p6mm$ [7,8,30,33-35].

In order to make a Fourier series expansions, we recall that for group $p6mm$ with hexagonal lattice the spatial periods $\boldsymbol{a}_{1(2)}$ have equal lengths, $\left|\boldsymbol{a}_{1(2)}\right| = \lambda$, and are inclined relative to one another at the angle $2\pi/3$, with $\boldsymbol{a}_1 \cdot \boldsymbol{a}_2 = -1/2$, Figure 3. Their coordinates in the (x,y) plane are $\boldsymbol{a}_1 = (1,0)\lambda$ and $\boldsymbol{a}_2 = \left(-1/2, \sqrt{3}/2\right)\lambda$. The wave-vectors $\boldsymbol{k}_{1(2)}$ of the reciprocal lattice are defined by the relations $\boldsymbol{k}_{1(2)} \cdot \boldsymbol{a}_{2(1)} = 0$ and $\boldsymbol{k}_{1(2)} \cdot \boldsymbol{a}_{1(2)} = 2\pi$, leading to $\boldsymbol{k}_1 = \left(\sqrt{3}/2, 1/2\right)k$ and $\boldsymbol{k}_2 = (0,1)\,k$ with $k = 4\pi/\left(\lambda\sqrt{3}\right)$ and $\boldsymbol{k}_1 \cdot \boldsymbol{k}_2 = 1/2$ [7,8,24,25,30,33-35]. Linear combination of independent spatial periods $\boldsymbol{a}_{1(2)}$ defines the spatial period $\boldsymbol{a}_3 = -\left(\boldsymbol{a}_1 + \boldsymbol{a}_2\right)$, whereas linear combination of independent wave-vectors of the reciprocal lattice $\boldsymbol{k}_{1(2)}$ defines the wavevector $\boldsymbol{k}_3 = \boldsymbol{k}_1 - \boldsymbol{k}_2$ with $\boldsymbol{k}_3 = \left(\sqrt{3}/2, -1/2\right)k$, Figure 3. The wave-vectors $\boldsymbol{k}_{1(2)}$ (as well as wave-vectors $\boldsymbol{k}_{1(3)}$) are inclined relative to one another at the angle $\pi/3$, Figure 3 [7,8,24,25,30,33].

The Fourier series expansions of the potentials $\Phi_{h(l)}$ have the form:

$$\Phi_h(\boldsymbol{r},z,t) = \sum_{m=0}^{\infty}\Phi_m(t)\left(z + \frac{exp(-mkz)}{3mk}\sum_{i=1}^{3}cos\left(m\boldsymbol{k}_i\boldsymbol{r}\right)\right) + f_h(t) + cross\ terms,$$

$$\Phi_l(\boldsymbol{r},z,t) = \sum_{m=0}^{\infty}\tilde{\Phi}_m(t)\left(-z + \frac{exp(mkz)}{3mk}\sum_{i=1}^{3}cos\left(m\boldsymbol{k}_i\boldsymbol{r}\right)\right) + f_l(t) + cross\ terms \qquad (4.1)$$

Here $\boldsymbol{r} = (x,y)$, $\Phi_m\left(\tilde{\Phi}_m\right)$ are the Fourier amplitudes of the heavy (light) fluid with $\Phi_0 = \tilde{\Phi}_m = 0$, $f_{h(l)}$ are time-dependent functions, and m is integer [7,8,30,34]. Cross terms appear in high orders. These Fourier series expansions hold true upon transformations of the group $p6mm$, including the rotations on angles $\pm\pi/3, \pm 2\pi/3, \pm\pi$ with the axis of rotation in the z-direction, and the reflections $x \to -x$, $y \to -y$ as well as $(x,y) \to -(x,y)$ in the mirror reflection planes along the x- and y- directions:

$$\sum_{i=1}^{3} cos(m\boldsymbol{k}_i\boldsymbol{r}) = cos(m\boldsymbol{k}_1\boldsymbol{r}) + cos(m\boldsymbol{k}_2\boldsymbol{r}) + cos(m\boldsymbol{k}_3\boldsymbol{r}) =$$
$$\left(cos\left(mk\left(\frac{\sqrt{3}}{2}x + \frac{1}{2}y \right) \right) + cos\left(mk\left(\frac{\sqrt{3}}{2}x - \frac{1}{2}y \right) \right) + cos(mk\, y) \right) \qquad (4.2)$$

The fluid interface is $\theta = -z + z^*(\mathbf{r}, t)$, and function $z^*(\mathbf{r}, t)$ is defined locally as

$$z^*(\boldsymbol{r}, t) = \sum_{N=1}^{\infty} \hat{\zeta}_N(t) \sum_{i=1}^{3} (\boldsymbol{k}_i\boldsymbol{r})^{2i} + cross\ terms \quad (5.1)$$

and with account for

$$\sum_{i=1}^{3} (\boldsymbol{k}_i\boldsymbol{r})^2 = (\boldsymbol{k}_1\boldsymbol{r})^2 + (\boldsymbol{k}_2\boldsymbol{r})^2 + (\boldsymbol{k}_3\boldsymbol{r})^2 =$$
$$k^2\left(\left(\frac{\sqrt{3}}{2}x + \frac{1}{2}y \right)^2 + \left(\frac{\sqrt{3}}{2}x - \frac{1}{2}y \right)^2 + y^2 \right) = \frac{3}{2}k^2(x^2 + y^2) \qquad (5.2)$$

to

$$z^* = \sum_{N=1}^{\infty} \zeta_N(t)(x^2 + y^2)^{2N} + cross\ terms \quad (5.3)$$

Here N is natural, ζ_N are the surface variables, $\zeta_1 = \zeta$ is the principal curvature at the bubble (spike) tip. Cross terms appear in high orders.

The solution is sought for $t > 0$, and, as time evolves, with $\zeta \le 0, v \ge 0$ for bubbles, and $\zeta \ge 0, v \le 0$ for spikes.

Sub-section 2.4 – Dynamical system for group *p6mm*

Upon substituting these expansions in the governing equations and further expanding the equations in the vicinity of the bubble tip, we derive from the governing equations a dynamical system in terms of moments and surface variables. For group p6mm, to first order $N = 1$, the interface is $z^* = \zeta(x^2 + y^2)$, and the dynamical system is [7,8,24,30]:

$$M_0 = -\tilde{M}_0 = -v, \quad \rho_h\left(\dot{\zeta} - 2\zeta M_1 - \frac{M_2}{4} \right) = 0, \quad \rho_l\left(\dot{\zeta} - 2\zeta \tilde{M}_1 + \frac{\tilde{M}_2}{4} \right) = 0,$$
$$\rho_h\left(\frac{\dot{M}_1}{4} + \zeta \dot{M}_0 - \frac{M_1^2}{8} + \zeta g \right) = \rho_l\left(\frac{\dot{\tilde{M}}_1}{4} - \zeta \dot{\tilde{M}}_0 - \frac{\tilde{M}_1^2}{8} + \zeta g \right), \quad M_1 - \tilde{M}_1 = arbitrary \qquad (6.1)$$

These equations represent the absence of mass sources, the continuity of the normal component of velocities and the normal component of momentum at the interface, and the discontinuity of the tangential component of velocity at the interface. Values $M\left(\widetilde{M}\right)$ are the moments, with

$$M_n = \sum_{m=0}^{\infty} \Phi_n k^n m^n + cross\ terms, \quad \widetilde{M}_n = \sum_{m=0}^{\infty} \widetilde{\Phi}_n k^n m^n + cross\ terms \qquad (6.2)$$

with integer n.

Section 3 - Results

Sub-section 3.1 – Early-time dynamics

For the early-time dynamics only the first order harmonics are retained in the expressions for the momentum, $M_n = k^n \Phi_1$, $\widetilde{M}_n = k^n \widetilde{\Phi}_1$, $n = 0,1,2$, transforming the dynamical system to:

$$M_0 = -\widetilde{M}_0 = -v, \quad \rho_h\left(\dot{\zeta} - 2\zeta k M_0 - k^2 \frac{M_0}{4}\right) = 0, \rho_l\left(\dot{\zeta} - 2\zeta k \widetilde{M}_0 + k^2 \frac{\widetilde{M}_0}{4}\right) = 0,$$

$$\rho_h\left(k^2 \frac{\dot{M}_0}{4} + \zeta \dot{M}_0 - k^2 \frac{M_0^2}{8} + \zeta g\right) = \rho_l\left(k^2 \frac{\dot{\widetilde{M}}_0}{4} - \zeta \dot{\widetilde{M}}_0 - k^2 \frac{\widetilde{M}_0^2}{8} + \zeta g\right),$$

$$M_0 - \widetilde{M}_0 = arbitrary \qquad (7)$$

The initial conditions at time t_0 are the initial curvature $\zeta_0 = \zeta(t_0)$ and velocity $v(t_0)$. The latter sets the initial growth-rate $v_0 = |v(t_0)|$. For a given wavelength λ and for $a \neq -2$, there are two time-scales in the dynamics, $\tau_G = (kG)^{-1/(a+2)}$ and $\tau_0 = (kv_0)^{-1}$. At $a = -2$ the time-scale is $\tau_0 = (kv_0)^{-1}$, and the acceleration strength is parameterized by the value (Gk). We consider dynamics for $t_0 > \{\tau_G, \tau_0\}$.

For a broad class of initial conditions, integration of the governing equations is a challenge [24]. The solution can be found when the initial perturbation amplitude is small and the interface is nearly flat, $|\zeta/k| << 1$, particularly, $|\zeta/k| << 1/8$ (hence $<< 1/4$). Indeed, for $|\zeta/k| << 1/8$ in Eqs.(7), with $|2\zeta k M_0| << |k^2 M_0/4|$ and $|2\zeta k \widetilde{M}_0| << |k^2 \widetilde{M}_0/4|$, the equations for the continuity of the normal component of velocities at the interface are transformed to

$$\rho_h\left(\dot{\zeta} - 2\zeta k M_0 - k^2 M_0/4\right) = 0 \quad \Rightarrow \quad \rho_h\left(\dot{\zeta} - k^2 M_0/4\right) = 0$$
$$\rho_l\left(\dot{\zeta} - 2\zeta k \widetilde{M}_0 + k^2 \widetilde{M}_0/4\right) = 0 \quad \Rightarrow \quad \rho_l\left(\dot{\zeta} + k^2 \widetilde{M}_0/4\right) = 0$$

For $\left|\zeta/k\right| << 1/4$ in Eqs.(7) with $\left|k^2\,\dot{M}_0/4\right| >> \left|\zeta\dot{M}_0\right|$ and $\left|k^2\,\dot{\tilde{M}}_0/4\right| >> \left|\zeta\dot{\tilde{M}}_0\right|$, the equation for the continuity of the normal component of momentum at the interface is transformed to

$$\rho_h\left(k^2\,\dot{M}_0/4+\zeta\dot{M}_0-k^2\,M_0^2/8+\zeta g\right)=\rho_l\left(k^2\,\dot{\tilde{M}}_0/4-\zeta\dot{\tilde{M}}_0-k^2\,\tilde{M}_0^2/8+\zeta g\right)\;\Rightarrow$$

$$\rho_h\left(k^2\,\dot{M}_0/4-k^2\,M_0^2/8+\zeta g\right)=\rho_l\left(k^2\,\dot{\tilde{M}}_0/4-k^2\,\tilde{M}_0^2/8+\zeta g\right)$$

With account for that $M_0=-\tilde{M}_0=-v$ and $v^2=M_0^2=\tilde{M}_0^2$, the system Eqs.(7) is transformed to

$$\dot{\zeta}+\left(\frac{k^2}{4}\right)v=0,\quad \dot{v}+\left(\frac{Ak}{2}\right)v^2+\left(\frac{4A}{k}\right)\zeta G t^a=0 \quad (8)$$

Note that the term involving v^2 should be kept since it defines the time scale at $g=0$ [22-24,31].

Consider the dynamics for $a\neq -2$. With $\sigma=-(\zeta/k), V=v/v_0$, $T=t/\tau_s$, where τ_s is some time-scale, the system gets the form

$$\frac{d^2\sigma}{dT^2}-A\left[\sigma T^a\left(\frac{\tau_s}{\tau_G}\right)^{a+2}-2\left(\frac{d\sigma}{dT}\right)^2\right]=0,\quad \left(\frac{d\sigma}{dT}\right)-\left(\frac{\tau_s}{\tau_0}\right)\frac{V}{4}=0 \quad (9)$$

This system indicates the existence of two distinct sub-regimes depending on the interplay of the acceleration parameters and the initial growth-rate – the acceleration-driven (Rayleigh-Taylor type) sub0regime and the initial growth-rate driven (Richtmyer-Meshkov type) sub-regime. Indeed, with $\tau_s=\tau_0$, we find from the first equation in the system, see Figure 4:

$$\left(\frac{\tau_0}{\tau_G}\right)^{a+2}>>2 \;\Leftrightarrow\; \left(\frac{\tau_0}{\tau_G}\right)>>2^{\frac{1}{a+2}} \;\Rightarrow\; \left(\frac{\tau_0}{\tau_G}\right)<<1 \quad \text{for} \quad a>-2 \quad (10.1)$$

$$\left(\frac{\tau_0}{\tau_G}\right)^{a+2}<<2 \;\Leftrightarrow\; \left(\frac{\tau_0}{\tau_G}\right)<<2^{\frac{1}{a+2}} \;\Rightarrow\; \left(\frac{\tau_0}{\tau_G}\right)<<1 \quad \text{for} \quad a<-2 \quad (10.2)$$

Sub-section 3.2 – Solutions for early-time dynamics

Sub-section 3.2.1 – Acceleration exponents greater than -2

For $a>-2$ the smallest time-scale is τ_G, $\tau_G<<\tau_0$, the relative contribution of the terms is $\left|\sigma T^a\left(\tau_0/\tau_G\right)^{a+2}\right| >> \left|2\left(d\sigma/dT\right)^2\right|$, and the dynamics is driven by the acceleration (and is Rayleigh-Taylor type). With the time-scale of the fastest process $\tau_s=\tau_G$, the system is transformed to

$$\frac{d^2\sigma}{dT^2} - A\left[\sigma T^a\right] = 0, \quad V - 4\left(\frac{\tau_0}{\tau_G}\right)\frac{d\sigma}{dT} = 0 \quad (11.1)$$

The solution of the system is

$$\sigma = C_1\sqrt{T}\, I_{\frac{1}{2s}}\left(\sqrt{A}\frac{T^s}{s}\right) + C_2\sqrt{T}\, I_{-\frac{1}{2s}}\left(\sqrt{A}\frac{T^s}{s}\right), \quad V = 4\left(\frac{\tau_0}{\tau_G}\right)\frac{d\sigma}{dT} \quad (11.2)$$

where $s = (a+2)/2$ and I_p is the modified Bessel function of the pth order. In complete agreement with the classic results, for constant acceleration, $a = 0$, the solution is transformed to

$$\sigma = C_1\, exp\left(\sqrt{A}T\right) + C_2\left(-\sqrt{A}T\right), \quad V = 4\left(\frac{\tau_0}{\tau_G}\right)\frac{d\sigma}{dT} \quad (11.3)$$

In the dimensional form with $\tau_G = (kG)^{-1/(a+2)}$ the solution is

$$\left(-\frac{\zeta}{k}\right) = C_1\sqrt{\frac{t}{\tau_G}}\, I_{\frac{1}{2s}}\left(\sqrt{A}\frac{(t/\tau_G)^s}{s}\right) + C_2\sqrt{\frac{t}{\tau_G}}\, I_{-\frac{1}{2s}}\left(\sqrt{A}\frac{(t/\tau_G)^s}{s}\right), \quad v = \frac{4}{k}\frac{d(-\zeta/k)}{dt} \quad (11.4)$$

Table 1 summarizes these results. Figure 5 illustrates the solutions in Eqs.(11) for bubbles with $\zeta \le 0, v \ge 0$ and spikes with $\zeta \ge 0, v \le 0$ at various values of the acceleration exponents.

Sub-section 3.2.2 – Acceleration exponents smaller than -2

For $a < -2$ the smallest time-scale is τ_0, $\tau_0 << \tau_G$, the relative contribution of the terms is $\left|\sigma T^a(\tau_0/\tau_G)^{a+2}\right| << \left|2(d\sigma/dT)^2\right|$, and the dynamics is driven by the initial growth-rate (and is Richtmyer-Meshkov type). With the time-scale of the fastest process $\tau_s = \tau_0$, the system is transformed to

$$\frac{d^2\sigma}{dT^2} + 2A\left(\frac{d\sigma}{dT}\right)^2 = 0, \quad V - 4\left(\frac{d\sigma}{dT}\right) = 0 \quad (12.1)$$

The solution of the system is

$$\sigma = \frac{ln(C_2T + C_1)}{2A}, \quad V = 4\left(\frac{d\sigma}{dT}\right) \quad (12.2)$$

or, in the dimensional form

$$\left(-\frac{\zeta}{k}\right) = \frac{ln(C_2(t/\tau_0) + C_1)}{2A}, \quad v = \frac{4}{k}\frac{d(-\zeta/k)}{dt} \quad (12.3)$$

Table 2 summarizes these results. Figure 6 illustrates the solutions in Eqs.(12) for bubbles with $\zeta \le 0, v \ge 0$ and spikes with $\zeta \ge 0, v \le 0$ at various values of the acceleration exponents.

Sub-section 3.2.3 – Acceleration exponent -2

At $a=-2$, the acceleration is $g=Gt^{-2}$, the time-scale is $\tau_0=(kv_0)^{-1}$, the acceleration strength is parameterized by (Gk), and the system is transformed to

$$\frac{d^2\sigma}{dT^2}-A\left[\sigma\frac{Gk}{T^2}-2\left(\frac{d\sigma}{dT}\right)^2\right]=0,\quad \frac{d\sigma}{dT}-\frac{V}{4}=0 \quad (13)$$

For strong acceleration $Gk>>1$ with terms related as $\left|\sigma T^{-2}(Gk)\right|>>\left|2(d\sigma/dT)^2\right|$, the dynamics is acceleration-driven, and the system is transformed to

$$\frac{d^2\sigma}{dT^2}-\sigma\frac{AGk}{T^2}=0,\quad \frac{d\sigma}{dT}-\frac{V}{4}=0 \quad (14.1)$$

The solution of the system is

$$\sigma=C_1T^{p_1}+C_2T^{p_2},\quad p_{1,2}=\left(1\pm\sqrt{1+4AGk}\right),\qquad V=4\frac{d\sigma}{dT} \quad (14.2)$$

In the limiting case of strong acceleration $AGk>>1$

$$\sigma=C_1T^{p}+C_2T^{-p},\quad p=\sqrt{4AGk},\qquad V=4\frac{d\sigma}{dT} \quad (14.3)$$

and, in the dimensional form, the solution is

$$\left(-\frac{\zeta}{k}\right)=C_1\left(\frac{t}{\tau_0}\right)^{p}+C_2\left(\frac{t}{\tau_0}\right)^{-p},\quad p=\sqrt{4AGk},\quad v=\frac{4}{k}\frac{d(-\zeta/k)}{dt} \quad (14.4)$$

For weak acceleration $Gk<<1$ with terms related as $\left|\sigma T^{-2}(Gk)\right|<<\left|2(d\sigma/dT)^2\right|$, the dynamics is driven by the initial growth-rate, and the system is transformed to

$$\frac{d^2\sigma}{dT^2}+2A\left(\frac{d\sigma}{dT}\right)^2=0,\quad V-4\frac{d\sigma}{dT}=0 \quad (15.1)$$

The solution of the system in the dimensionless and dimensional forms is

$$\sigma=\frac{ln(C_2T+C_1)}{2A},\quad V=4\frac{d\sigma}{dT} \quad (15.2)$$

$$\left(-\frac{\zeta}{k}\right)=\frac{ln(C_2(t/\tau_0)+C_1)}{2A},\quad v=\frac{4}{k}\frac{d(-\zeta/k)}{dt} \quad (15.3)$$

Table 3 presents solutions in the limiting cases of strong and weak accelerations. Figure 7 illustrates the solutions in Eqs.(14) and Eqs.(15) for bubbles with $\zeta\le 0, v\ge 0$ and spikes with $\zeta\ge 0, v\le 0$ at various values of the acceleration strength.

Sub-section 3.2.4 – Very early time dynamics

For very early time dynamics with very short time intervals, $(t-t_0)/t_0 << 1$ and $t_0 > \{\tau_G, \tau_0\}$, the governing equations can be linearized. By using the sign function sgn, the solution is

$$\zeta - \zeta(t_0) = -\frac{k^2}{4} v_0 (t-t_0) sgn\left[\frac{v(t_0)}{v_0}\right], \quad v - v(t_0) = -\left(\frac{Ak}{2} v_0^2 + \frac{4A}{k} \zeta_0 G t_0^a\right)(t-t_0) \quad (16)$$

in full consistency with the foregoing results [23,24]. Table 4 summarizes these results.

Section 3.3 - Effect of initial conditions

Our general solutions are applicable for any sign of $\zeta_0 k$ and $v(t_0)/v_0$. To study qualitatively how the bubbles and spikes are being formed in the early time dynamics [7,8,31], we represent the short time interval solution, for $0 < (t-t_0)/t_0 << 1$ with $t_0 >> \{\tau_G, \tau_0\}$, in the form

$$\zeta - \zeta(t_0) = -\frac{k}{4}\left[\frac{t-t_0}{\tau_0}\right] sgn\left[\frac{v(t_0)}{v_0}\right],$$
$$v - v(t_0) = -\frac{A}{2} v_0 \left[\frac{t-t_0}{\tau_0}\right] - 4A \frac{(\zeta_0/k)^{-1}}{(\tau_G k)} \left(\frac{t_0}{\tau_G}\right)^a \left[\frac{t-t_0}{\tau_G}\right] \quad (17)$$

Two sub-regimes are clearly seen from this expression: the acceleration-driven (Rayleigh-Taylor type) sub-regime, with $\tau_G/\tau_0 << 1$ and $|v_0(\tau_G/\tau_0)| << |8(\zeta_0/k)(\tau_G k)^{-1}(t_0/\tau_G)^a|$, and the initial growth-rate-driven (Richtmyer-Meshkov type) sub-regime, with $\tau_0/\tau_G << 1$ and $|v_0(\tau_G/\tau_0)| >> |8(\zeta_0/k)(\tau_G k)^{-1}(t_0/\tau_G)^a|$.

In the acceleration-driven regime, $\tau_G/\tau_0 << 1$, the morphology and the velocity of the interface near the tip change with time as follows: For $v(t_0)/v_0 > 0$ and $\zeta_0 k < 0$, the interface becomes more curved and its velocity increases, since $(\zeta - \zeta(t_0))/k < 0, (v - v(t_0))(\tau_G k) > 0$. For $v(t_0)/v_0 > 0$ and $\zeta_0 k > 0$, the interface flattens and the velocity decreases, $(\zeta - \zeta(t_0))/k < 0, (v - v(t_0))(\tau_G k) < 0$. For $v(t_0)/v_0 < 0$ and $\zeta_0 k > 0$, the interface becomes more curved and the velocity magnitude increases, $(\zeta - \zeta(t_0))/k > 0, (v - v(t_0))(\tau_G k) < 0$. For $\zeta_0 k < 0$ and $v(t_0)/v_0 < 0$, the interface flattens and the velocity magnitude decreases, $(\zeta - \zeta(t_0))/k > 0, (v - v(t_0))(\tau_G k) > 0$. This suggests that the bubbles are formed at the regular points of the interface with $\zeta_0 k < 0$, whereas the spikes are formed at the

regular points of the interface with $\zeta_0 k > 0$. In the acceleration-driven (Rayleigh-Taylor type) dynamics, the positions of the bubbles and spikes are set by the initial morphology of the interface.

In the initial growth-rate driven regime, $\tau_0/\tau_G << 1$, the morphology and the velocity of the interface near the tip change with time as follows: For $v(t_0)/v_0 > 0$ and $\zeta_0 k < 0$, the interface becomes more curved and its velocity decreases, since $(\zeta - \zeta(t_0))/k < 0, (v - v(t_0))(\tau_G k) < 0$. For $v(t_0)/v_0 > 0$ and $\zeta_0 k > 0$, the interface flattens and velocity decreases, $(\zeta - \zeta(t_0))/k < 0, (v - v(t_0))(\tau_G k) < 0$. For $v(t_0)/v_0 < 0$ and $\zeta_0 k > 0$, the interface becomes more curved and velocity magnitude increases, since $(\zeta - \zeta(t_0))/k > 0, (v - v(t_0))(\tau_G k) > 0$. For $v(t_0)/v_0 < 0$ and $\zeta_0 k < 0$, the interface flattens and the velocity magnitude increases, $(\zeta - \zeta(t_0))/k > 0, (v - v(t_0))(\tau_G k) < 0$. This suggests that the bubbles are formed at the regular points of the interface with $v(t_0)/v_0 > 0$, and the spikes are formed at the regular points of the interface with $v(t_0)/v_0 > 0$. In the initial growth-rate driven (Richtmyer-Meshkov type) dynamics, the positions of the bubbles and spikes are set by the initial velocity field.

Figure 8 presents the schematics of the effect of initial conditions on the early time dynamics and illustrates the process of formation of bubbles and spikes.

Sub-section 3.4 - Theory benchmarks

According to our results, for variable acceleration with power-law time-dependence, for the acceleration exponents $a > -2$ and at $a = -2, Gk >> 1$, the early time dynamics is driven by the acceleration and the positions of the bubbles and spikes are set by the interface morphology, similarly to the case of RTI with constant acceleration. Hence we call the acceleration-driven dynamics as being 'RT-type' [3,4,7,9,10,29,31]. For the acceleration exponents $a < -2$ and at $a = -2, Gk << 1$, the early time dynamics is driven by the initial growth-rate and the positions of the bubbles and spikes are set by the initial velocity field. This dynamics is similar to the case of the Richtmyer-Meshkov instability, where the growth of the interface perturbation is due to impulsive acceleration by the shock; in a broad parameter regime the initial growth-rate is constant and the associated motion is nearly incompressible. Hence we call the initial-growth-rate-driven dynamics as being 'RM-type' [4,5,7,10,16,29,31].

Note that in the RTI and RMI in supernova blasts and in ICF environments, typical values of the acceleration exponents are $a > -2$ [17,18,24,26] According to our results, while in these cases the acceleration is usually induced by unsteady shocks, the early time dynamics of the unstable flow is RT-type: It is defined by the acceleration parameters, with the positions of bubbles and spikes set by the initial morphology of the interface [3,4,7,9,10,29,31].

Our results identify theory benchmarks for experiments and simulations, which, to our knowledge, have not been discussed before [7-24]. Specifically, by implementing in experiments and simulations an acceleration with exponents $a > -2$ one can study RT-type dynamics, and observe super-exponential growth of the interface perturbations for $a > 0$ and sub-exponential growth for $-2 < a < 0$, Figure 4, Figure 5. By implementing in experiments and simulations an accelerations with exponents $a < -2$ one can study RM-type dynamics, and observe the growth of the interface perturbations, which is set by the initial growth-rate and is independent of the exponent, Figure 4, Figure 6. By implementing an acceleration with exponent $a = -2$, one can further observe the effect of the acceleration strength on the dynamics, Figure 4, Figure 7.

In addition to quantitative study of dependence of the instability growth-rate on the acceleration parameters and the initial growth-rate, one can investigate the dependence of the unstable dynamics on the initial conditions. Particularly, for RT-type dynamics, one can observe that the formation of bubbles and spikes structure is prescribed by the morphology of the initially perturbed interface, Figure 8. This result is in excellent agreement with experiments [9-16,29]. For RM-type dynamics, one can further observe that the process of formation of the structure of bubbles and spikes is prescribed by the initial velocity field at the interface, Figure 8. For some initial conditions, it may lead to the so-called 'phase reversal', with bubbles (spikes) turning to spikes (bubbles), in excellent agreement with experiments and simulations [12,29,31].

The other important diagnostic parameter found by our theory is the qualitative velocity field [23,24]. According to our results in RT- and RM-type dynamics the non-equilibrium velocity field is characterized by effectively no motion of the fluids away from the interface, intensive motion of the fluids in a vicinity of the interface, and the production of shear-driven vortical structures at small scales at the interface, Figure 9 [7,8,23,24,30]. This result excellently agrees with experiments and simulations [9-16]. Note that for a shock-induced acceleration, the non-equilibrium velocity is referred to the velocity in a frame of reference moving with the velocity of the background motion [5,6,12,10,16]. This is because for a spatially extended periodic flow the post-shock dynamics is a superposition of two motions – the background motions of the fluids and the interface in the transmitted shock direction, and the growth of the interface perturbations due to impulsive acceleration by the shock. The velocity scale of the background motion is substantially greater than the initial growth-rate; for strong shock the former is usually super-sonic, whereas the latter is sub-sonic [16].

Our analysis can be applied for three-dimensional flows with other symmetries and two-dimensional flow [7,8,24,33]. Particularly, for three-dimensional highly symmetric flows, the dynamics is universal, except for the difference in the wavevector value for a given λ [7,8,30]. This universality is due to a nearly isotropic character of the dynamics in the plane normal to the acceleration [7,8,30].

Section 4 – Discussion

We have studied the long-standing problem of the early-time dynamics of Rayleigh-Taylor instability with time-variable acceleration and for a spatially extended three-dimensional flow periodic in the plane normal to the acceleration with symmetry group p6mm, Eqs.(1-17). For the acceleration with power-law time-dependence, $g = Gt^a$, by employing group theory and scaling analysis, we have explicitly found the instability growth-rate in a broad range of the acceleration parameters, have investigated the dependence of the dynamics on the initial conditions, and have elaborated theory benchmarks. Two distinct sub-regimes of the early time dynamics, depending on the acceleration exponent, have been discovered. To our knowledge, these findings have not been discussed in details before [1-35].

Particularly, we have found that for exponents $a > -2$, the time-scale is $\tau_G = (kG)^{-1/(a+2)}$, and the dynamics is of the acceleration-driven RT-type, Eqs.(11). For exponents $a < -2$, the time-scale is $\tau_0 = (kv_0)^{-1}$, and the dynamics is of the initial growth-rate driven RM-type, Eqs.(12). At the exponent $a = -2$, the time-scale is $\tau_0 = (kv_0)^{-1}$, and the dynamics changes its character from RT to RM-type with decrease of the acceleration strength Gk, Eqs.(14,15) For very early time dynamics, the solution depends linearly on the short time interval, Eqs.(16). The formation of the structure of bubbles and spikes is prescribed by the initial morphology of the interface for RT-type dynamics, and by the initial velocity field for RM-type dynamics, Eqs.(17).

Our results are in excellent agreement with available experiments and simulations [9-17,24,29], and elaborate theory benchmarks for future experiments and simulations. These include the dependence of the instability growth-rate on the acceleration parameters and the initial growth-rate, the dependence of the process of formation of the structure of bubbles and spikes on the initial morphology of the interface and the initial velocity filed, along with qualitative properties of non-equilibrium flow fields, including the intense motions of the fluids near the interface and effectively no motion of the fluids away from the interface.

Our analysis can be extended to study advanced stages of RTI and RT mixing [24], and to systematically account for the properties of non-ideal fluids, including the effects of compressibility, surface tension, and viscosity [10-20,27,28], to be done in future research. By further applying the multi-scale method for scale-dependent RT dynamics with variable acceleration, one can conduct a scrupulous quantitative study of the effect of initial conditions on the acceleration-driven RT-type dynamics, and the effect of acceleration on the initial growth-rate driven RM-type dynamics, to be done in future research.

Finally note that our analysis is of particular interest for the studies of RT-relevant phenomena under conditions of high energy density, such as supernova or fusion, where the instability is often driven

by explosions or implosions with acceleration exponents set by blast waves or impact waves [24]. In this case the exponent value is $-2 < a < -1$, and the dynamics is RT-type in the early-time scale-dependent regime and is RM-type in the self-similar mixing regime [24]. Accurate numerical modeling and experimental diagnostics of RT dynamics for $-2 < a < -1$ is a challenge requiring extensive theory benchmarks [24]. Our results suggest that in addition to a direct comparison of experiments and simulations with the theory for a particular exponent a, one can also conduct a comparative study of RT dynamics for various values of acceleration exponents [24]. Specifically, since for variable acceleration $g = Gt^a$ the instability growth-rate in the early-time regime is given by tabular special functions, such as modified Bessel functions, an excellent performance of numerical codes and experimental diagnostics in the case of 'fast' dynamics with exponents $a > -1$ may provide more confidence in their performance in the case of 'slow' dynamics with exponents $a \in (-2,-1)$ under conditions relevant for a supernova [24].

Section 5 - Acknowledgements

SIA thanks the University of Western Australia (AUS) for financial support under the project grant 10101047 and the National Science Foundation (USA) for financial support under the award 1404449. The authors' contributions to this work are as follows: DLH conducted analytical studies. AKB made plots for Figures 5,6,7. SIA conducted analytical studies and led the project, including its scientific and organizational aspects.

Section 6 - References

1. Abarzhi SI, Gauthier S, Sreenivasan KR (2013) Turbulent mixing and beyond: non-equilibrium processes from atomistic to astrophysical scales. I,II. Royal Society Publishing, ISBN 1782520384, ISBN 0854039864.
2. Abarzhi SI, Sreenivasan KR (2010) Turbulent mixing and beyond. Royal Society Publishing ISBN 085403806X.
3. Rayleigh Lord (1883) Investigations of the character of the equilibrium of an incompressible heavy fluid of variable density. Proc London Math Soc 14:170-177.
4. Davies RM & Taylor GI (1950) The mechanics of large bubbles rising through extended liquids and through liquids in tubes. Proc R Soc A 200:375-390.
5. Richtmyer RD (1960) Taylor instability in shock acceleration of compressible fluids. Commun Pure Appl Math 13:297-319.
6. Meshkov EE (1969) Instability of the interface of two gases accelerated by a shock. Sov Fluid Dyn 4:101-104.
7. Abarzhi SI (2010) Review of theoretical modeling approaches of Rayleigh-Taylor instabilities and turbulent mixing. Phil Trans R Soc A 368:1809-1828.
8. Abarzhi SI (2008) Review of nonlinear dynamics of the unstable fluid interface: conservation laws and group theory. Phys Scr 2008:014012..
9. Anisimov SI, Drake RP, Gauthier S, Meshkov EE, Abarzhi SI (2013) What is certain and what is not so certain in our knowledge of Rayleigh–Taylor mixing? Phil Trans R Soc A 371:20130266.
10. Meshkov EE (2013) Some peculiar features of hydrodynamic instability development. Phil Trans R Soc A 371:20120288.
11. Kadau K, Barber JL, Germann TC, Holian BL, Alder BJ (2010) Atomistic methods in fluid simulation. Phil Trans R S:368,1547.
12. Nishihara K, Wouchuk JG, Matsuoka C et al (2010) Richtmyer–Meshkov instability: theory of linear and nonlinear evolution. Phil Trans R Soc A 368:1769-1807.
13. Gauthier S, Le Creurer B (2010) Compressibility effects in Rayleigh-Taylor instability-induced flows. Phil Trans R Soc A 368:1681.
14. Glimm J, Sharp DH, Kaman T, Lim H (2013) New directions for Rayleigh–Taylor mixing. Phil Trans R Soc A 371:20120183.
15. Robey HF, Zhou Y, Buckingham AC, Keiter P, Remington BA, Drake RP (2003) The time scale for the transition to turbulence in a high Reynolds number, accelerated flow. Phys Plasmas 10, 614.
16. Dell Z et al (2017) Maximum initial growth-rate of strong-shock-driven Richtmyer-Meshkov instability. Phys Plasmas 24:090702.
17. Haan SW et al (2011) Point design targets, specifications, and requirements for the 2010 ignition campaign on the National Ignition Facility. Phys Plasmas:18,051001.
18. Arnett D 1996 Supernovae and Nucleosynthesis. Princeton University Press. ISBN 9780691011479.
19. Peters N 2000 Turbulent Combustion. Cambridge University Press.
20. Rana S, Herrmann M (2011) Primary atomization of a liquid jet in crossflow. Phys Fluids:23,091109.
21. Buehler MJ, Tang H, van Duin ACT, Goddard WA (2007) Threshold Crack Speed Controls Dynamical Fracture of Silicon Single Crystals Phys Rev Lett:99,165502
22. Swisher N, Kuranz C, Arnett WD et al (2015) Rayleigh-Taylor mixing in supernova experiments. Phys Plasmas 22:102707.
23. Bhowmick AK, Abarzhi SI (2016) Richtmyer-Meshkov unstable dynamics influenced by pressure fluctuations. Phys Plasmas 23:111610.
24. Abarzhi SI, Bhowmick AK, Naveh A, Pandian A, Swisher NC, Stellingwerf RF, Arnett WD (2018) Supernova, nuclear synthesis, fluid instabilities and interfacial mixing. Proc Natl Acad Sci USA 201714502.
25. Landau LD, Lifshitz EM (1987) Theory Course I-X, Pergamon Press, New York.
26. Sedov L (1993) Similarity and dimensional methods in mechanics. CRC Press. 10th ed.
27. Chandrasekhar S 1961 Hydrodynamic and Hydromagnetic Stability. London: Oxford University Press.
28. Kull HJ (1991) Theory of Rayleigh-Taylor instability. Phys Rep 206:197.
29. Meshkov EE 2006 Studies of hydrodynamic instabilities in laboratory experiments, Sarov, FGYC-VNIIEF, ISBN 5-9515-0069-9 (in Russian).
30. Abarzhi SI (1998) Stable steady flows in Rayleigh–Taylor instability. Phys Rev Lett 81:337–40.
31. Abarzhi SI (2000) Regular and singular late-time asymptotes of potential motion of fluid with a free-boundary. Phys Fluids 12:3112.
32. Ilyin DV, Fukumoto Y, Goddard WA, Abarzhi SI (2018) Analysis of dynamics, stability, and flow fields' structure of an accelerated hydrodynamic discontinuity with interfacial mass flux by a general matrix method. Phys Plasmas **25**, 112105
33. Shubnikov AV, Koptsik VA 1974 Symmetry in science and art. Springer. ISBN 978-1468420692.
34. Abarzhi SI (2008) Coherent structures and pattern formation in the Rayleigh-Taylor turbulent mixing, Physica Scripta 78, 015401.
35. Cosgrove JM, Forbes LK (2017) A delta-plane simulation of anticyclones perturbing circumpolar flows to form a transient north polar hexagon. Mon Not R Astron Soc 469, 4133.

Section 7 – Tables

Table 1: Solutions for early-time dynamics of Rayleigh-Taylor type for Rayleigh-Taylor instability with variable acceleration $g = Gt^a$

Early-time dynamics of Rayleigh-Taylor type		
a	τ	Solution
$a > -2$	$\tau = \tau_G$ $\tau_G = (kG)^{-1/(a+2)}$	$\left(-\frac{\zeta}{k}\right) = C_1\sqrt{\frac{t}{\tau_G}}\, I_{\frac{1}{2s}}\left(\sqrt{A}\,\frac{(t/\tau_G)^s}{s}\right) + C_2\sqrt{\frac{t}{\tau_G}}\, I_{-\frac{1}{2s}}\left(\sqrt{A}\,\frac{(t/\tau_G)^s}{s}\right)$, $v = \frac{4}{k}\frac{d(-\zeta/k)}{dt}$

Table 2: Solutions for early-time dynamics of Richtmyer-Meshkov type for Rayleigh-Taylor instability with variable acceleration $g = Gt^a$

Early-time dynamics of Richtmyer-Meshkov type		
a	τ	Solution
$a < -2$	$\tau = \tau_0$ $\tau_0 = (kv_0)^{-1}$	$\left(-\frac{\zeta}{k}\right) = \frac{ln(C_2(t/\tau_0)+C_1)}{2A}$, $v = \frac{4}{k}\frac{d(-\zeta/k)}{dt}$ (12.3)

Table 3: Solutions for early-time dynamics of Rayleigh-Taylor type and Richtmyer-Meshkov type for Rayleigh-Taylor instability with variable acceleration $g = Gt^a$

Early-time dynamics of Rayleigh-Taylor type and Richtmyer-Meshkov type		
$a = -2$	$\tau = \tau_0$ $\tau_0 = (kv_0)^{-1}$	Solution
$a = -2$ $Gk >> 1$	Rayleigh-Taylor type	$\left(-\frac{\zeta}{k}\right) = C_1\left(\frac{t}{\tau_0}\right)^{\sqrt{4AGk}} + C_2\left(\frac{t}{\tau_0}\right)^{-\sqrt{4AGk}}$, $v = \frac{4}{k}\frac{d(-\zeta/k)}{dt}$
$Gk << 1$	Richtmyer-Meshkov type	$\left(-\frac{\zeta}{k}\right) = \frac{ln(C_2(t/\tau_0)+C_1)}{2A}$, $v = \frac{4}{k}\frac{d(-\zeta/k)}{dt}$

Table 4: Solutions for very early-time dynamics of Rayleigh-Taylor type and Richtmyer-Meshkov type for Rayleigh-Taylor instability with variable acceleration $g = Gt^a$

Very early time dynamics of Rayleigh-Taylor type and Richtmyer-Meshkov type		
$\forall a$	$(t-t_0)/t_0 << 1$ $t_0 >> \{\tau_G, \tau_0\}$ $\tau_G = (kG)^{-1/(a+2)}$ $\tau_0 = (kv_0)^{-1}$	$\zeta - \zeta(t_0) = -\frac{k}{4}\left[\frac{t-t_0}{\tau_0}\right] sgn\left[\frac{v(t_0)}{v_0}\right]$, $v - v(t_0) = -\frac{A}{2}v_0\left[\frac{t-t_0}{\tau_0}\right] - 4A\frac{(\zeta_0/k)}{(\tau_G k)}\left(\frac{t_0}{\tau_G}\right)^a\left[\frac{t-t_0}{\tau_G}\right]$

Section 8 –Figures captions and Figures

Figure 1: Schematics of large-scale coherent structure of bubbles and spikes in Rayleigh-Taylor instability. Arrows mark directions of the fluid motion near the tip of the bubble (up) and spike (down). Small-scale shear-driven interfacial vortical structures (not shown) may result in a mushroom shape of the spike.

Figure 2: Sample patterns for (a) a one-dimensional space group in a two-dimensional flow and (b) two-dimensional space groups of square and hexagon in a three-dimensional flow.

Figure 3: Two-dimensional space groups of hexagon with (a) group generators; (b) spatial period vectors of the hexagonal lattice and wave-vectors of the reciprocal lattice.

Figure 4: Acceleration exponents for the early time dynamics of Rayleigh-Taylor instability with variable acceleration of (top) acceleration-driven Rayleigh-Taylor (RT) type and (bottom) initial growth-rate-driven Richtmyer-Meshkov type.

Figure 5: Solutions for the early-time dynamics of acceleration-driven Rayleigh-Taylor (RT) type with exponents greater than -2 for Rayleigh-Taylor instability with variable acceleration.

Figure 6: Solutions for the early-time dynamics of initial growth-rate-driven Richtmyer-Meshkov type with exponents smaller than -2 for Rayleigh-Taylor instability with variable acceleration.

Figure 7: Solutions for the early-time dynamics of acceleration-driven Rayleigh-Taylor (RT) type and initial growth-rate-driven Richtmyer-Meshkov (RM) type at exponent -2 and transition between sub-regimes with varying the acceleration strength for Rayleigh-Taylor instability with variable acceleration.

Figure 8: Schematics of the effect of initial conditions on the interface evolution in Rayleigh-Taylor instability with variable acceleration of (top) Rayleigh-Taylor (RT) type and (bottom) Richtmyer-Meshkov (RM) type.

Figure 9: Qualitative fields of the velocity, the velocity streamlines and the interface perturbation in the plane along the acceleration for the early-time Rayleigh-Taylor instability with variable acceleration. Each plot has its own range of values to better illustrate the plot features.

Fig. 1

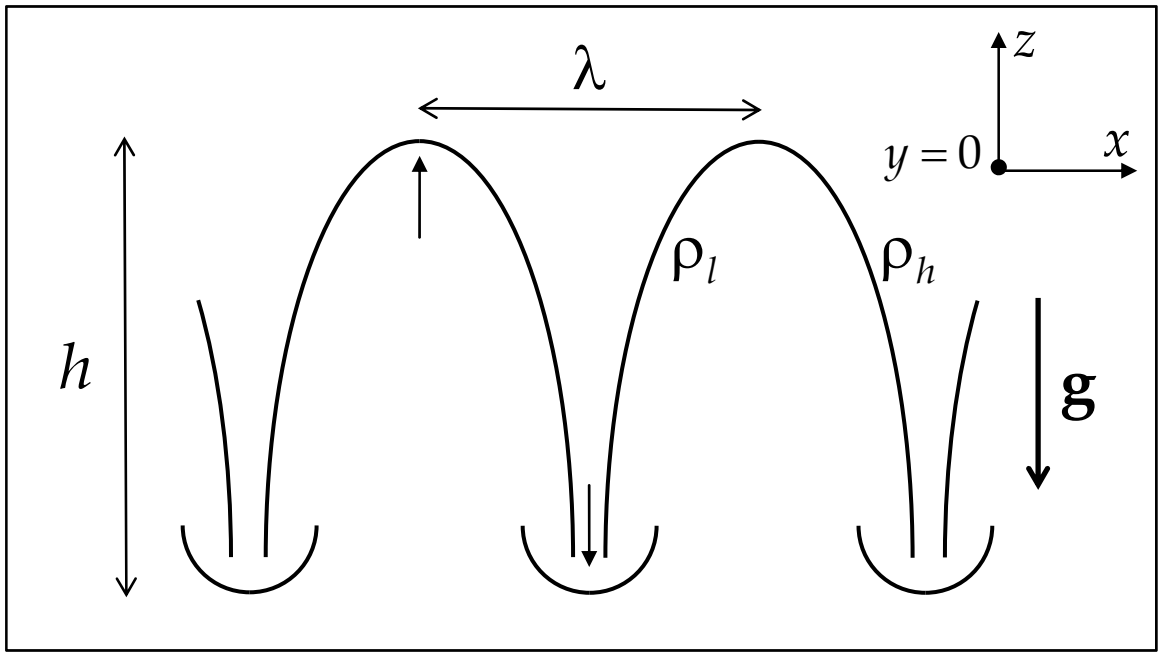

Fig. 2

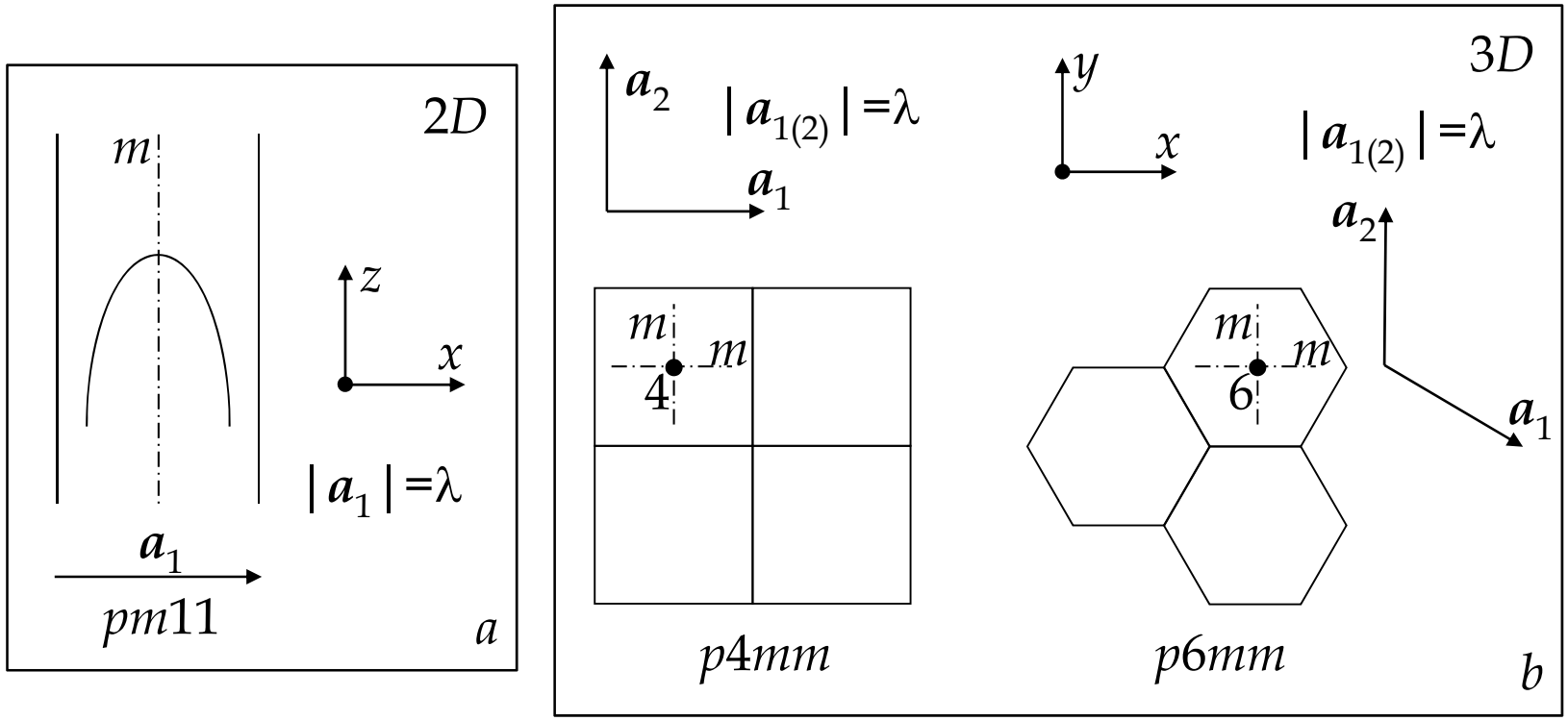
2D
m
z
x
| a1 | =λ
a1
pm11
a
3D
a2
| a1(2) | =λ
a1
y
x
| a1(2) | =λ
a2
m
m
4
p4mm
m
m
6
a1
p6mm
b

Fig. 3

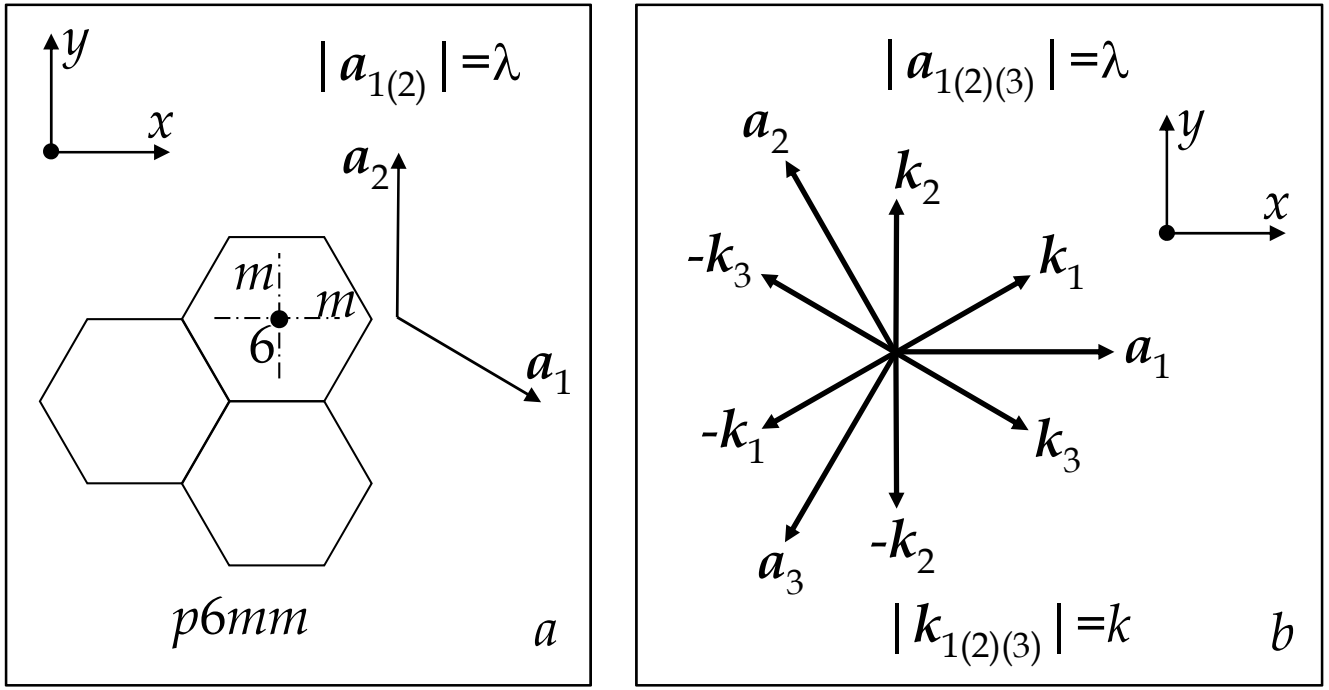

Fig. 4

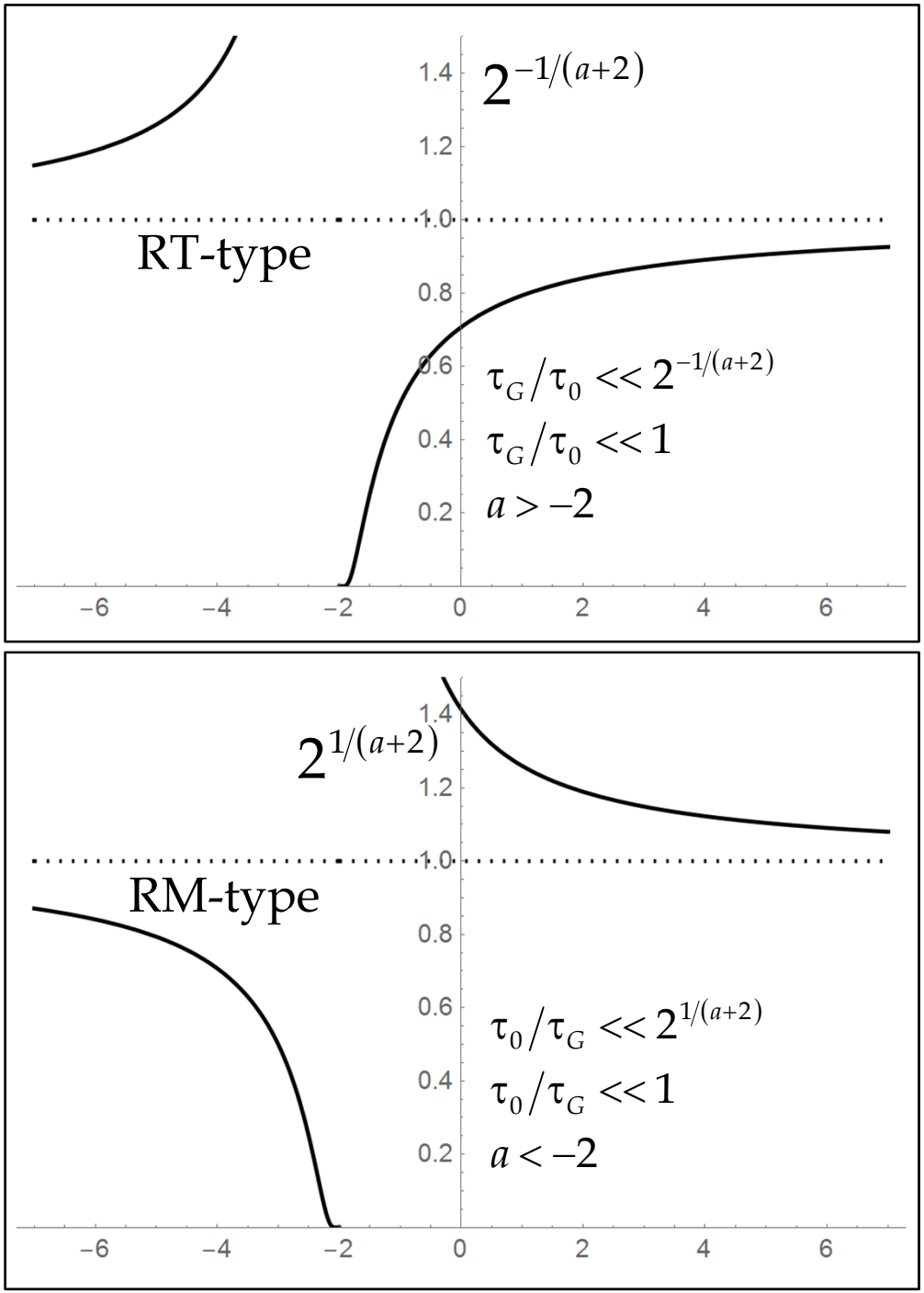
$2^{-1/(a+2)}$
RT-type
$\tau_G/\tau_0 << 2^{-1/(a+2)}$
$\tau_G/\tau_0 << 1$
$a > -2$
$2^{1/(a+2)}$
RM-type
$\tau_0/\tau_G << 2^{1/(a+2)}$
$\tau_0/\tau_G << 1$
$a < -2$
1.4
1.2
1.0
0.8
0.6
0.4
0.2
−6
−4
−2
0
2
4
6

Fig. 5

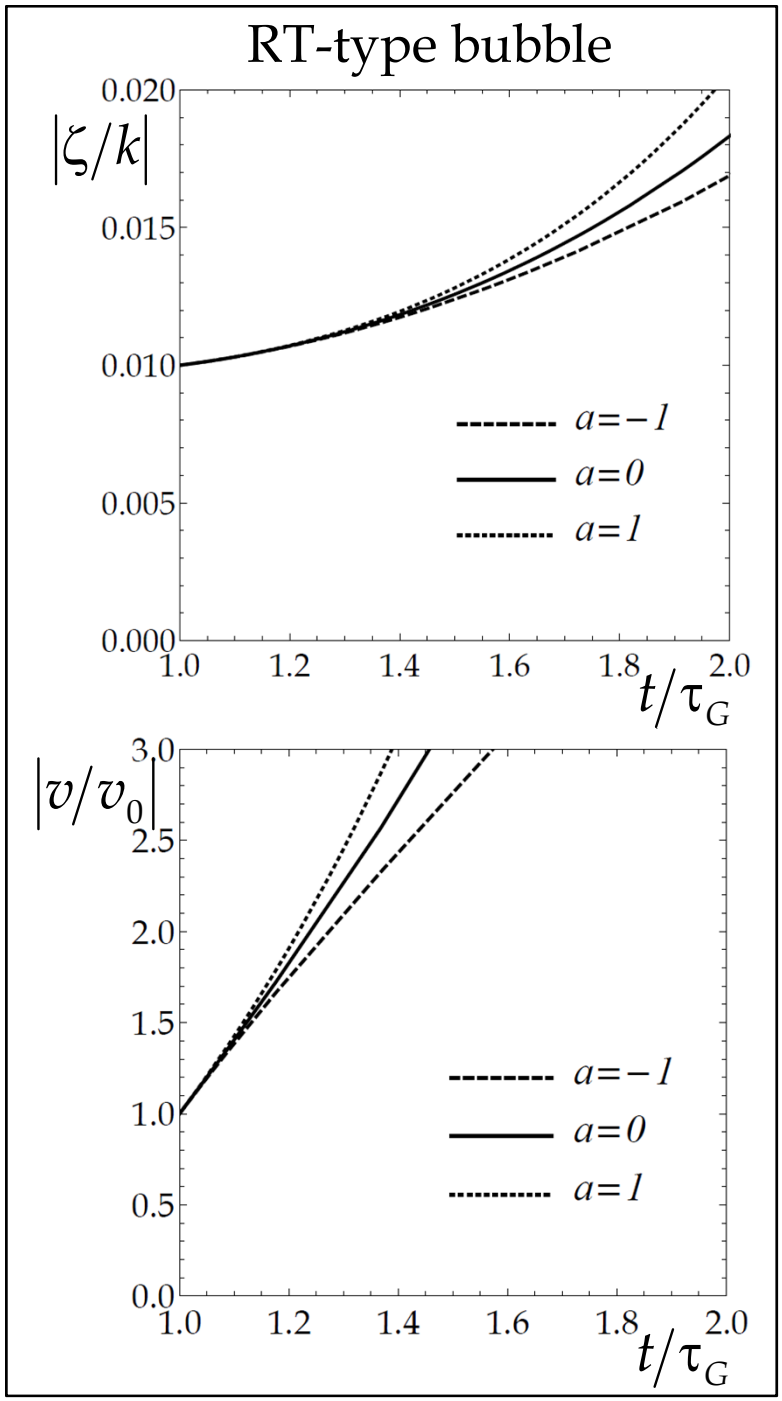
RT-type bubble
$|\zeta/k|$
0.020
0.015
0.010
0.005
0.000
1.0
1.2
1.4
1.6
1.8
2.0
t/τ_G
$a=-1$
$a=0$
$a=1$
$|v/v_0|$
3.0
2.5
2.0
1.5
1.0
0.5
0.0
1.0
1.2
1.4
1.6
1.8
2.0
t/τ_G
$a=-1$
$a=0$
$a=1$

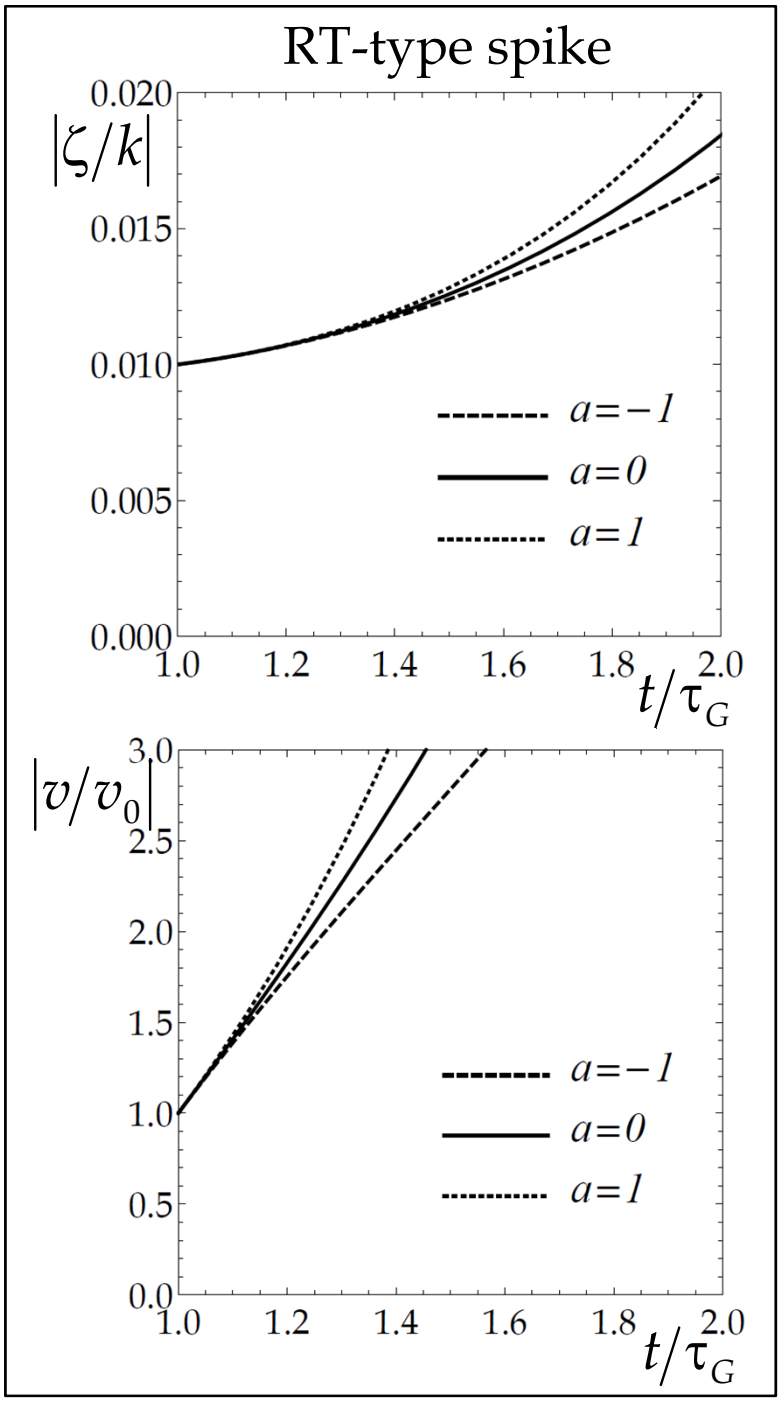
RT-type spike
$|\zeta/k|$
0.020
0.015
0.010
0.005
0.000
1.0
1.2
1.4
1.6
1.8
2.0
t/τ_G
$a=-1$
$a=0$
$a=1$
$|v/v_0|$
3.0
2.5
2.0
1.5
1.0
0.5
0.0
1.0
1.2
1.4
1.6
1.8
2.0
t/τ_G
$a=-1$
$a=0$
$a=1$

Fig. 6

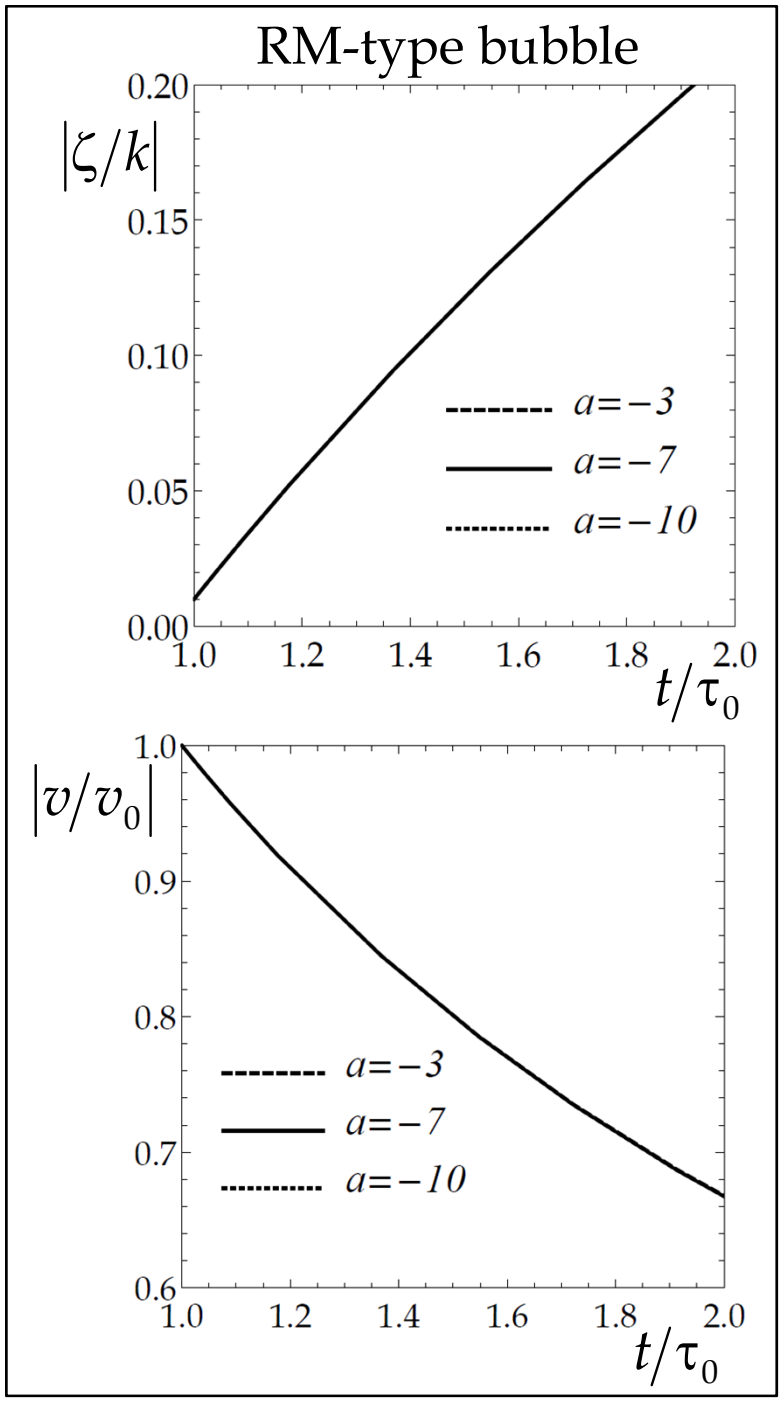
RM-type bubble
$|\zeta/k|$
0.20
0.15
0.10
0.05
0.00
1.0
1.2
1.4
1.6
1.8
2.0
t/τ_0
$a=-3$
$a=-7$
$a=-10$
$|v/v_0|$
1.0
0.9
0.8
0.7
0.6
1.0
1.2
1.4
1.6
1.8
2.0
t/τ_0
$a=-3$
$a=-7$
$a=-10$

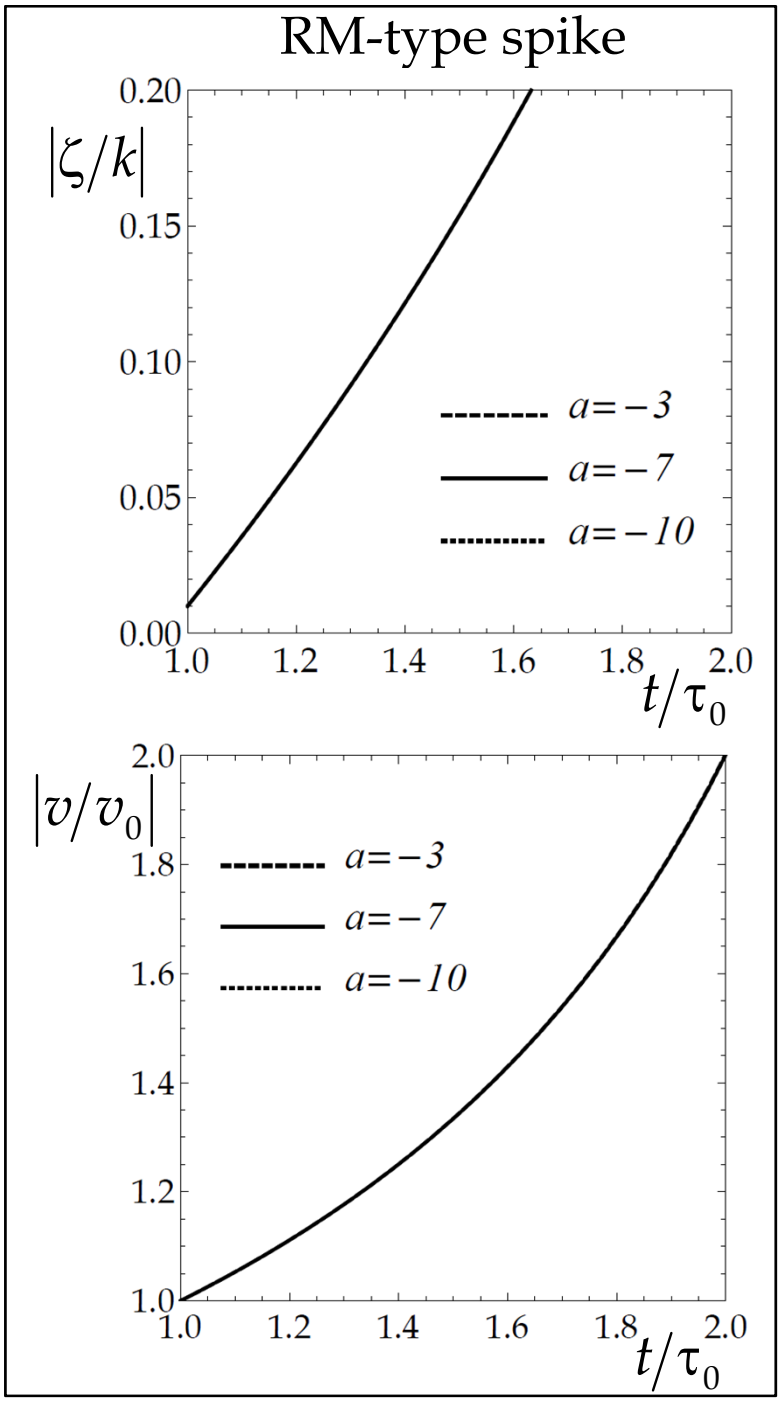
RM-type spike
$|\zeta/k|$
0.20
0.15
0.10
0.05
0.00
1.0
1.2
1.4
1.6
1.8
2.0
t/τ_0
$a=-3$
$a=-7$
$a=-10$
$|v/v_0|$
2.0
1.8
1.6
1.4
1.2
1.0
1.0
1.2
1.4
1.6
1.8
2.0
t/τ_0
$a=-3$
$a=-7$
$a=-10$

Fig. 7

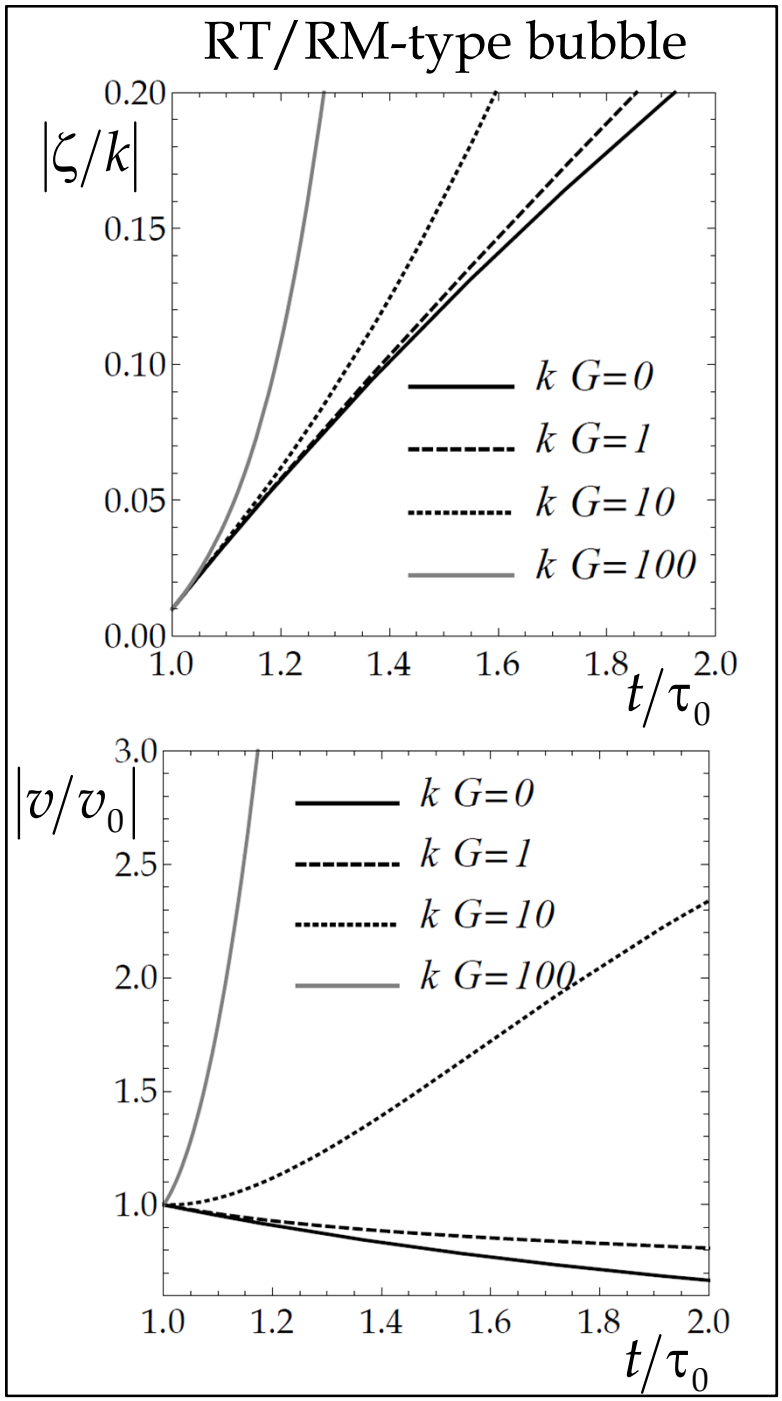
RT/RM-type bubble
$|\zeta/k|$
0.20
0.15
0.10
0.05
0.00
1.0
1.2
1.4
1.6
1.8
2.0
t/τ_0
k G=0
k G=1
k G=10
k G=100
$|v/v_0|$
3.0
2.5
2.0
1.5
1.0
1.0
1.2
1.4
1.6
1.8
2.0
t/τ_0
k G=0
k G=1
k G=10
k G=100

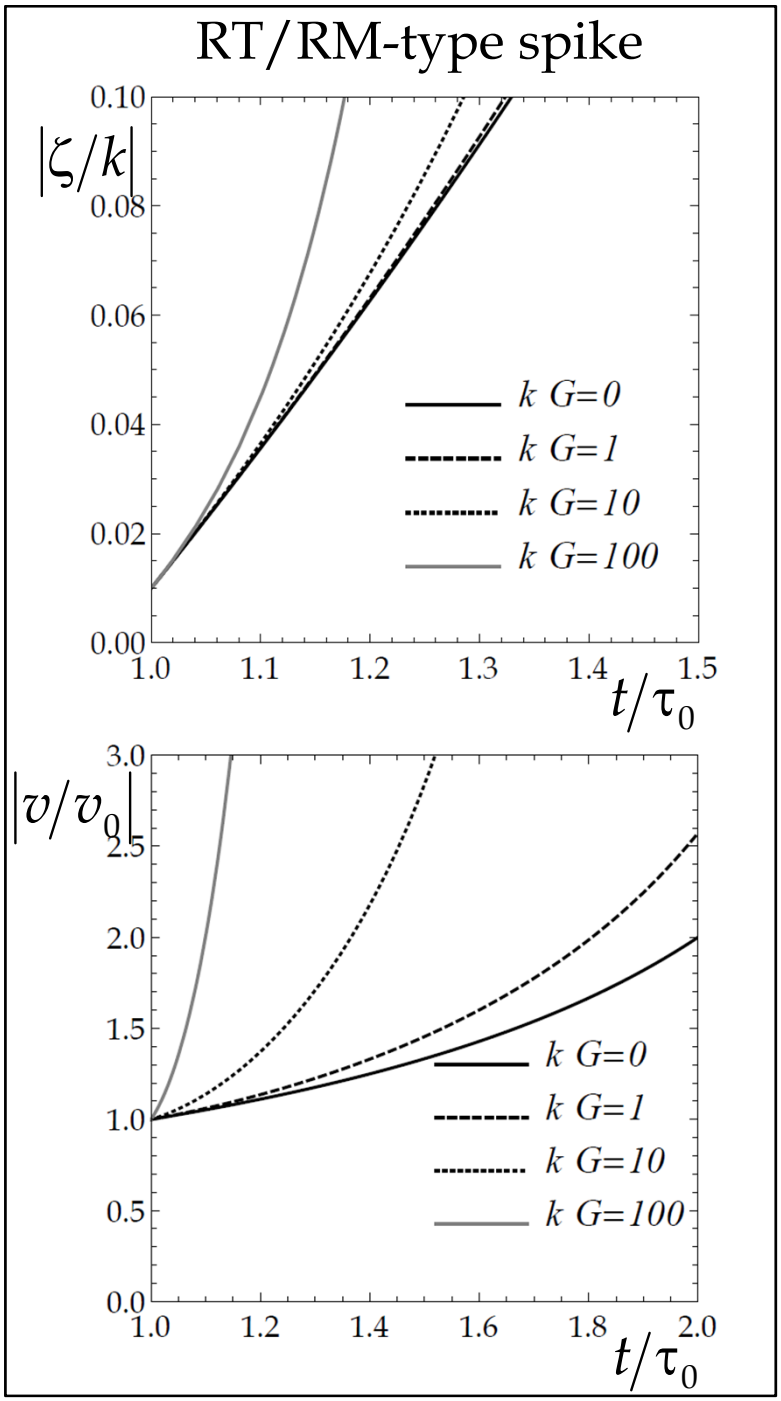
RT/RM-type spike
$|\zeta/k|$
0.10
0.08
0.06
0.04
0.02
0.00
1.0
1.1
1.2
1.3
1.4
1.5
t/τ_0
k G=0
k G=1
k G=10
k G=100
$|v/v_0|$
3.0
2.5
2.0
1.5
1.0
0.5
0.0
1.0
1.2
1.4
1.6
1.8
2.0
t/τ_0
k G=0
k G=1
k G=10
k G=100

Fig. 8

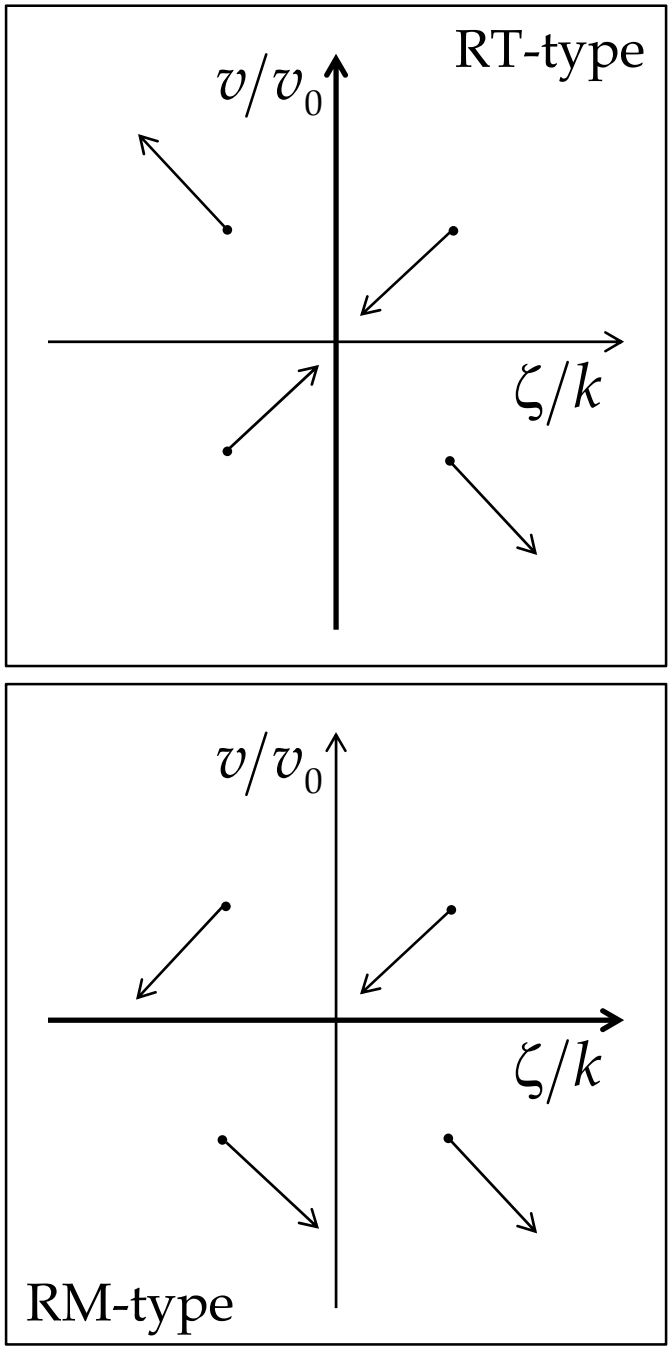

Fig. 9

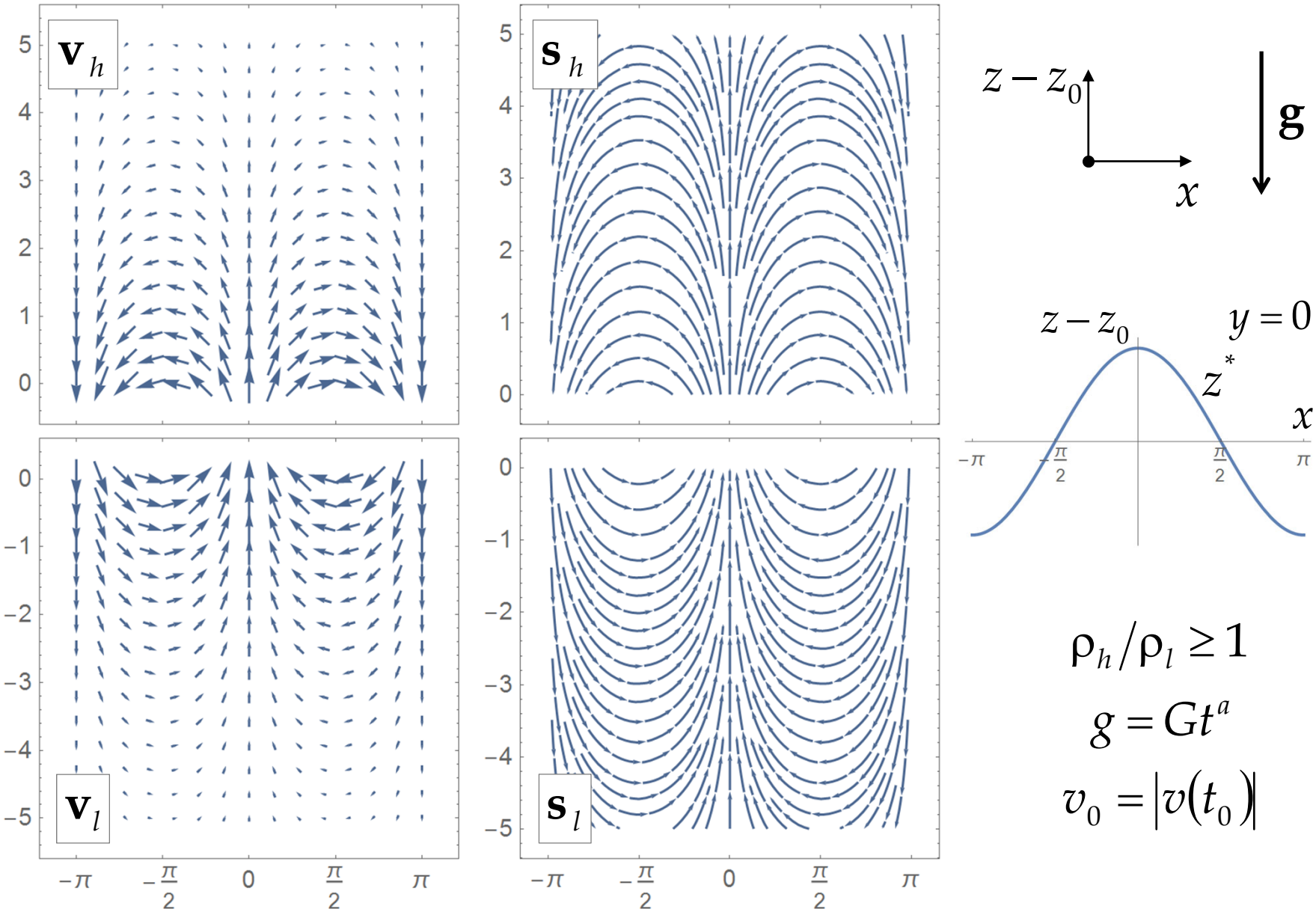
$\mathbf{v}_h$
$\mathbf{s}_h$
$\mathbf{v}_l$
$\mathbf{s}_l$
$z - z_0$
x
$\mathbf{g}$
$z - z_0$
$y = 0$
z^*
x
$\rho_h / \rho_l \geq 1$
$g = Gt^a$
$v_0 = |v(t_0)|$